

On the phase description of chaotic oscillators

Takashi Imai,^{1,*} Hiromichi Suetani,^{2,3} and Toshio Aoyagi¹

¹Graduate School of Informatics, Kyoto University, Kyoto 606-8501, Japan

²Faculty of Science and Technology, Oita University, Oita 870-1192, Japan

³Rhythm-Based Brain Information Processing Unit,

RIKEN Center for Brain Science, Saitama 351-0198, Japan

(Dated: May 12, 2022)

This paper presents a phase description of chaotic dynamics for the study of chaotic phase synchronization. A prominent feature of the proposed description is that it systematically incorporates the dynamics of the non-phase variables inherent in the system. Taking these non-phase dynamics into account is essential for capturing the complicated nature of chaotic phase synchronization, even in a qualitative manner. We numerically verified the validity of the proposed description for the Lorenz oscillator, and found that our method provides an accurate description of the characteristic distorted shape of the synchronization region of its chaotic oscillator.

The intrinsic rhythms exhibited by dynamical systems have attracted interest in a wide range of fields [1]. For example, the beating of the heart has been studied extensively, not only because of its importance with regard to human health, but also because it is a rich source of information as a dynamical system [2]. In many cases, such rhythmic systems interact with other oscillatory units, and these interactions create further intriguing phenomena. A typical example of such phenomena is phase synchronization [3], for example, synchronization between the heartbeat and locomotor rhythm [4], which is thought to improve the efficiency of blood circulation through active muscles.

The phase reduction approach provides a systematic method for analyzing phase synchronization [5]. This method provides a concise description of rhythm dynamics, and it has served as a framework for the study of phase synchronization for many years. In this way, the phase reduction approach has contributed greatly to our understanding of phase synchronization phenomena.

Although, in its conventional form, the phase reduction approach can be applied only to weakly perturbed limit-cycle oscillators, recently this approach has been extended to a more general form with broader application. For example, Refs. [6] and [7] demonstrate that phase reduction can be extended to noisy limit-cycle oscillators and limit-cycle solutions of reaction-diffusion systems, respectively. However, the application of phase reduction to the analysis of chaotic oscillators—a very common type of rhythmic system—has not yet been established.

For chaotic oscillators, the emergence of a variant of phase synchronization can often be found when the behavior of the system is described in terms of properly defined phase variables [8]. This type of synchronization phenomena exhibited by the phase variables in descriptions of chaotic dynamics is called *chaotic phase synchronization* (CPS). We believe that establishing the application of the phase reduction approach to the analysis of chaotic oscillators would lead to significant progress in our understanding of CPS. In this paper, we present

formalism that does indeed accomplish this.

A particularly difficult problem in formulating the phase reduction analysis of chaotic oscillators is to incorporate a proper treatment of the non-phase variables. For chaotic systems, in general, even a weak perturbation can cause a qualitative change in the behavior of the non-phase variables. Such changes may drastically alter the rhythmic properties of the oscillator. For this reason, it is important to properly treat the dynamics of the non-phase variables. However, in previous studies on the phase reduction of chaotic oscillators, this has not been done [9–11]. Contrastingly, in this paper we construct a phase description of chaotic dynamics that systematically incorporates the dynamics of the non-phase variables.

To derive a phase description of chaotic dynamics, first, we consider an unperturbed system of the form

$$\dot{X} = F(X), \quad X \in \mathbb{R}^m, \quad (1)$$

which we assume to possess a chaotic attractor. Let S be an $(m - 1)$ -dimensional surface of section. This surface can be partitioned into small cells, S_i . For each cell S_i , we choose a typical solution $X_r(t; i)$ of the differential equation (1), with the initial condition $X_r(0; i) \in S_i$. The solution $X_r(t; i)$ passes through the surface of section S repeatedly after the initial time ($t = 0$), and thus the time $T(i)$ of its first return to S can be defined (see Fig. 1). We call each trajectory $\Gamma_i := \{X_r(t; i) \mid 0 \leq t \leq T(i)\}$ the *representative trajectory* for the cell S_i , and we employ a set of the representative trajectories, $\{\Gamma_i\}$, as reference orbits for introducing a phase variable.

Suppose that in a neighborhood of the chaotic attractor, there exists a smooth change of coordinates $X \mapsto (R(X), \phi(X))$ satisfying the following conditions:

$$\begin{aligned} R(X) &\in \mathbb{R}^{m-1}, \quad \phi(X) \in [0, 2\pi], \\ \phi(X) &= 0 \iff X \in S, \end{aligned}$$

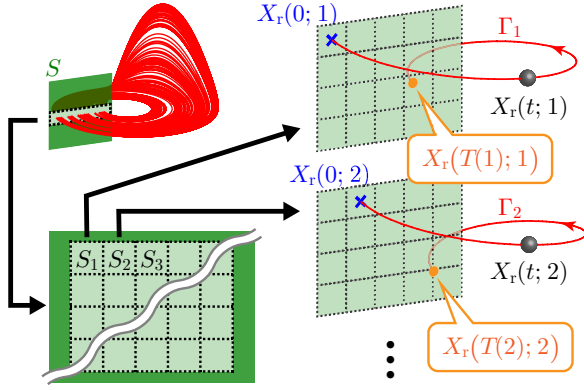


FIG. 1. (Color online) Construction of $\{S_i\}$ and $\{\Gamma_i\}$.

and

$$\frac{d\phi(X_r(t; i))}{dt} = \omega(i) := \frac{2\pi}{T(i)} \quad \text{if } 0 < t < T(i), \quad (2)$$

where the endpoints of the interval $[0, 2\pi]$ are identified with each other. Hereafter, we write $R(X(t))$ and $\phi(X(t))$ simply as $R(t)$ and $\phi(t)$. Although, in terms of the coordinates (R, ϕ) , the system (1) can be formally expressed as

$$\dot{R}(t) = F_R(R(t), \phi(t)), \quad \dot{\phi}(t) = F_\phi(R(t), \phi(t)), \quad (3)$$

it is more convenient to rewrite the latter in a phase-oscillator-like form. Let \mathcal{T}_n be the time of the n th return to S , and let \mathcal{C}_n be the index of the cell in which the state of the system exists at \mathcal{T}_n . For $t \in (\mathcal{T}_n, \mathcal{T}_{n+1}]$, the time evolution of ϕ can be expressed as follows:

$$\dot{\phi}(t) = \omega(\mathcal{C}_n) + \rho(R(t), \phi(t)). \quad (4)$$

When t passes \mathcal{T}_{n+1} (in other words, the next time the state returns to S), the evolution equation of ϕ is replaced with the new equation corresponding to the next cell, \mathcal{C}_{n+1} . The condition (2) implies the condition

$$\rho(R_r(t - \mathcal{T}_n; \mathcal{C}_n), \phi(t)) = 0, \quad (5)$$

where $R_r(t; i) := R(X_r(t; i))$.

Next, we consider the situation in which this oscillator is subject to a weak perturbation, $\varepsilon p(t)$, and the system is governed by the equation

$$\dot{X}(t) = F(X(t)) + \varepsilon p(t).$$

In this situation, the extent to which the time evolutions of R and ϕ are perturbed depends on sensitivity functions. Explicitly, these time evolutions are described by the following:

$$\dot{R}(t) = F_R(R(t), \phi(t)) + \varepsilon \left. \frac{\partial R(X)}{\partial X} \right|_{X=X(t)} p(t), \quad (6)$$

$$\begin{aligned} \dot{\phi}(t) &= \omega(\mathcal{C}_n) + \rho(R(t), \phi(t)) \\ &+ \varepsilon \text{grad}_X \phi(X)|_{X=X(t)} \cdot p(t). \end{aligned} \quad (7)$$

Let $\delta R(t)$ represent the deviation of $R(t)$ from its value on the representative trajectory; i.e., $\delta R(t) := R(t) - R_r(t - \mathcal{T}_n; \mathcal{C}_n)$ for $t \in (\mathcal{T}_n, \mathcal{T}_{n+1}]$. Here, we assume that the surface of section, S , is partitioned so finely that $\|\delta R(t)\|$ can be regarded as a small quantity of $\mathcal{O}(\varepsilon)$ until the next return to S . Ignoring terms of second and higher order with respect to ε and using the condition (5), we can rewrite Eqs. (6) and (7) as

$$\begin{aligned} \delta \dot{R}(t) &= \left. \frac{\partial F_R}{\partial R} \right|_{\substack{R=R_r(t-\mathcal{T}_n; \mathcal{C}_n) \\ \phi=\omega(\mathcal{C}_n)(t-\mathcal{T}_n)}} \delta R(t) \\ &+ \varepsilon \left. \frac{\partial R}{\partial X} \right|_{X=X_r(t-\mathcal{T}_n; \mathcal{C}_n)} p(t), \end{aligned} \quad (8)$$

$$\begin{aligned} \dot{\phi}(t) &= \omega(\mathcal{C}_n) + \left. \text{grad}_R \rho(R, \phi) \right|_{\substack{R=R_r(t-\mathcal{T}_n; \mathcal{C}_n) \\ \phi=\omega(\mathcal{C}_n)(t-\mathcal{T}_n)}} \cdot \delta R(t) \\ &+ \varepsilon \zeta(\omega(\mathcal{C}_n)(t - \mathcal{T}_n); \mathcal{C}_n) \cdot p(t), \end{aligned} \quad (9)$$

where

$$\zeta(\phi; i) := \text{grad}_X \phi(X)|_{X=X_r[\phi/\omega(i); i]}.$$

Define $\delta R_n := R_n - R_r(0; \mathcal{C}_n)$, where $R_n := R(\mathcal{T}_n)$. For $t \in (\mathcal{T}_n, \mathcal{T}_{n+1}]$, the differential equation (8) has the solution

$$\begin{aligned} \delta R(t) &= \Phi(t - \mathcal{T}_n; \mathcal{C}_n) \\ &\times \left[\delta R_n + \varepsilon \int_{\mathcal{T}_n}^t \Upsilon(s - \mathcal{T}_n; \mathcal{C}_n) p(s) ds \right], \end{aligned} \quad (10)$$

where $\Phi(\cdot; \mathcal{C}_n)$ is the fundamental matrix of the associated homogeneous equation whose value at the initial time, $\Phi(0; \mathcal{C}_n)$, is the identity matrix, and $\Upsilon(t; i) := \Phi^{-1}(t; i) (\partial R / \partial X)|_{X=X_r(t; i)}$. From Eq. (10), we obtain the recurrence equation

$$\begin{aligned} R_{n+1} &\simeq R_r(T(\mathcal{C}_n); \mathcal{C}_n) + \Phi(T(\mathcal{C}_n); \mathcal{C}_n) \left[\delta R_n \right. \\ &\left. + \varepsilon \int_{\mathcal{T}_n}^{\mathcal{T}_{n+1}} \Upsilon(t - \mathcal{T}_n; \mathcal{C}_n) p(t) dt \right]. \end{aligned} \quad (11)$$

The second term on the right-hand side of Eq. (9) represents the deviation of the frequency from its value on the representative trajectory, which is caused by $\delta R(t)$. Now, assume that the surface of section is selected to be one for which the variation in the return time is very small. Specifically, we assume that this variation is sufficiently small that the second term on the right-hand side of Eq. (9) is much smaller than the third term. Ignoring this small term, Eq. (9) can be rewritten as

$$\dot{\phi}(t) = \omega(\mathcal{C}_n) + \zeta(\phi(t); \mathcal{C}_n) \cdot p(t). \quad (12)$$

Equation (12) has the same form as the phase oscillator model, except for the \mathcal{C}_n -dependence. To remove the \mathcal{C}_n -dependence from Eq. (12), a bit more consideration is necessary. For simplicity, let us restrict the class of perturbation to periodic driving functions. With a weak periodic driving function $\varepsilon\tilde{p}(\theta)$ whose angular frequency, Ω , is close to the average frequency of the unperturbed system (1), the time evolution of the phase difference, $\psi(t) := \phi(t) - \Omega t$, will be much slower than that of $R(t)$. In this case, it is reasonable to regard ψ as a constant on the time scale of the R -dynamics. This allows us to reduce Eq. (11) to the map

$$R_{n+1} \simeq R_r(T(\mathcal{C}_n); \mathcal{C}_n) + \Phi(T(\mathcal{C}_n); \mathcal{C}_n) [\delta R_n + \varepsilon H(\mathcal{C}_n, \psi)], \quad (13)$$

where $H(i, \psi)$ denotes the averaged effect of the periodic driving:

$$H(i, \psi) = \frac{1}{\omega(i)} \int_0^{2\pi} \Upsilon \left[\frac{\phi}{\omega(i)}; i \right] \tilde{p}(\phi - \psi) d\phi.$$

The chaotic behavior of the system is encapsulated in the map (13). Iteration of Eq. (13) produces the (conditional) natural measure $\mu_i(\psi; \varepsilon)$ [12], the probability of visiting the cell S_i under the condition that the phase difference is equal to ψ . Averaging the ψ -dynamics with respect to μ_i , we obtain from Eq. (12) the flow described by

$$\dot{\psi}(t) = \delta\omega(\psi(t); \varepsilon) + \varepsilon G(\psi(t); \varepsilon), \quad (14)$$

where

$$\left. \begin{aligned} \delta\omega(\psi; \varepsilon) &:= \bar{\omega}(\psi; \varepsilon) - \Omega, & \bar{\omega}(\psi; \varepsilon) &:= \frac{2\pi}{\bar{T}(\psi; \varepsilon)}, \\ \bar{T}(\psi; \varepsilon) &:= \sum_i \mu_i(\psi; \varepsilon) T(i), \\ G(\psi; \varepsilon) &:= \frac{1}{2\pi} \int_0^{2\pi} \bar{\zeta}(\phi, \psi; \varepsilon) \cdot \tilde{p}(\phi - \psi) d\phi, \\ \bar{\zeta}(\phi, \psi; \varepsilon) &:= \sum_i \mu_i(\psi; \varepsilon) \frac{T(i)}{\bar{T}(\psi; \varepsilon)} \zeta(\phi; i). \end{aligned} \right\} \quad (15)$$

Note that this flow does not involve \mathcal{C}_n .

What does the existence of the flow described by Eq. (14) indicate? Note that Eq. (14) can be viewed as an averaged equation derived from the phase oscillator

$$\dot{\phi}(t) = \bar{\omega}(\psi; \varepsilon) + \varepsilon \bar{\zeta}(\phi(t), \psi; \varepsilon) \cdot \tilde{p}(\Omega t), \quad (16)$$

which is adjusted by the map (13) in the sense that $\bar{\omega}$ and $\bar{\zeta}$ depend on μ_i via Eqs. (15). In other words, the rhythmic dynamics of chaotic oscillators are described as a *map-adjusted phase oscillator* (MAPO). The existence of the flow described by Eq. (14) therefore indicates that the MAPO (16) with the map (13) determines the rhythmic

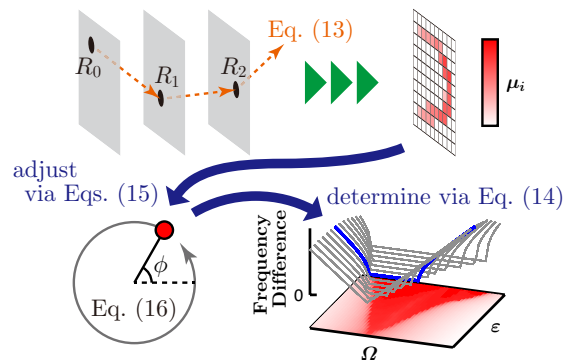


FIG. 2. (Color online) Representation using the map-adjusted phase oscillator (MAPO) model of how the rhythmic properties of the chaotic oscillator are determined.

properties (such as the average frequency) of the original chaotic oscillator, as illustrated in Fig. 2.

As a concrete example, let us consider the following Lorenz oscillator [13] driven by a weak sinusoidal perturbation:

$$\begin{aligned} \dot{x} &= \sigma(y - x) + \varepsilon \sin \Omega t, \\ \dot{y} &= x(\rho - z) - y, \quad \dot{z} = xy - \beta z, \end{aligned} \quad (17)$$

with the parameter values $\sigma = 10$, $\beta = 8/3$, and $\rho = 210$. We adopted a surface of section for which the variation in the return time is sufficiently small that Eq. (12) provides an accurate approximation of Eq. (9). (Details regarding the manner in which this surface was selected are presented in the Supplemental Material [14].) Using numerical simulations, we can easily evaluate $T(i)$, $R_r(T(i); i)$, $\Phi(T(i); i)$, $\Upsilon(t; i)$, and $\zeta(\phi; i)$. This allows us to calculate $\delta\omega$ and G defined in Eqs. (15). We smoothed the forms of $\delta\omega$ and G obtained in this manner by applying a moving average filter in the ψ direction [15]. With this treatment, the MAPO model produces the Arnold tongue that has almost the same shape as the tongue of the full model (17), as shown in Fig. 3.

The Arnold tongue of the Lorenz oscillator (17) has a peculiar shape, which differs from the triangular shape exhibited by the tongues of limit-cycle oscillators. Specifically, in the present case, the tongue has a horizontal plateau at $\varepsilon = \varepsilon_c \approx 0.46$. The origin of this plateau can be clarified through analysis of the MAPO model. In the region $\varepsilon > \varepsilon_c$, the map (13) has a wide periodic window over a certain range of ψ . The presence of this periodic window leads to large jumps in the value of $\delta\omega$ (see the insets of Fig. 3), which cause the extension of the synchronization range. This peculiar shape of the tongue of the Lorenz oscillator cannot be predicted from models proposed in the previous studies [9–11]. This example illustrates that the MAPO model helps us to understand the complicated nature of CPS.

The slight difference between the Arnold tongue obtained from the full model and that obtained from

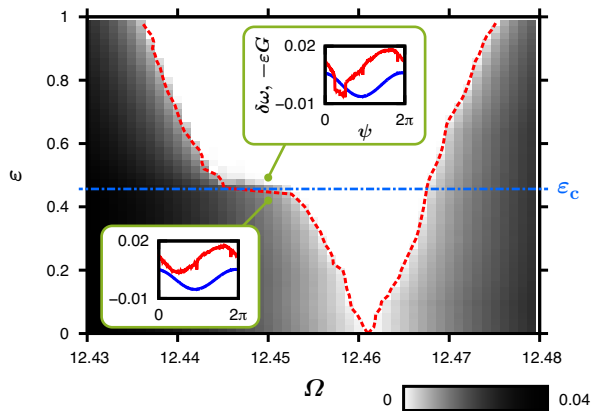


FIG. 3. (Color online) Numerical results for the Lorenz oscillator. The grayscale map depicts the difference between the frequencies of the periodic driving and the driven system observed in the full model. The dashed red curve indicates the edge of the Arnold tongue derived from the MAPO model (i.e., the boundary of the (ϵ, Ω) -region where CPS occurs in the MAPO model). The insets present representative examples of $\delta\omega$ (red curve) and $-\epsilon G$ (blue curve) calculated in the regions above and below $\epsilon = \epsilon_c$, where $\epsilon_c \approx 0.46$ is the value of ϵ at which the Arnold tongue of the Lorenz oscillator exhibits a horizontal plateau. The crossing of $\delta\omega$ and $-\epsilon G$ implies that CPS occurs at the values of ϵ and Ω used to plot their curves. (See the Supplemental Material [14] for the specific criteria used in this numerical demonstration.)

the MAPO model can be attributed to the anomalous enhancement of the diffusion coefficient discussed in Ref. [16]. We explain the effect of this enhancement in the Supplemental Material [14].

In summary, we have proposed the MAPO model as a framework for the study of CPS. This model consists of a chaotic map describing the evolution of the non-phase variables and a phase oscillator adjusted in accordance with the natural measure of the map, as illustrated in Fig. 2. This map, as well as the phase oscillator, depends on the perturbation applied to the original chaotic oscillator. Accordingly, the MAPO model allows us to examine how the perturbation induces a qualitative change in the behavior of the non-phase variables and alters the rhythmic properties of the chaotic oscillator.

Although in this paper we restricted the class of perturbation to external driving functions, our preliminary results (not shown here) suggest that the rhythm dynamics of mutually interacting chaotic oscillators can be also described as the MAPO model. Further analysis will be conducted in the near future.

This work was supported by MEXT KAKENHI Grant Numbers 15H05877, 26120006, and 25120011, and by JSPS KAKENHI Grant Numbers 16KT0019, 15587273, and 15KT0015.

* imai@acs.i.kyoto-u.ac.jp

- [1] A. A. Andronov, A. A. Vitt, and S. É. Khaikin, *Theory of Oscillators* (Pergamon Press, Oxford, 1966); P. Gray and S. K. Scott, *Chemical Oscillations and Instabilities: Nonlinear Chemical Kinetics* (Oxford University Press, New York, 1994); A. T. Winfree, *The Geometry of Biological Time* (Springer-Verlag, New York, 2001).
- [2] L. Glass and M. C. Mackey, *From Clocks to Chaos: The Rhythms of Life* (Princeton University Press, Princeton, 1988); L. Glass, Synchronization and rhythmic processes in physiology, *Nature* **410**, 277 (2001).
- [3] A. Pikovsky, M. Rosenblum, and J. Kurths, *Synchronization: A Universal Concept in Nonlinear Sciences* (Cambridge University Press, Cambridge, 2003).
- [4] R. L. Kirby, S. T. Nugent, R. W. Marlow, D. A. MacLeod, and A. E. Marble, Coupling of cardiac and locomotor rhythms, *Journal of Applied Physiology* **66**, 323 (1989); K. Niizeki, Intramuscular pressure-induced inhibition of cardiac contraction: implications for cardiac-locomotor synchronization, *American Journal of Physiology - Regulatory, Integrative and Comparative Physiology* **288**, R645 (2005).
- [5] A. T. Winfree, Biological rhythms and the behavior of populations of coupled oscillators, *Journal of Theoretical Biology* **16**, 15 (1967); Y. Kuramoto, *Chemical Oscillations, Waves, and Turbulence* (Springer-Verlag, Berlin, 1984); F. C. Hoppensteadt and E. M. Izhikevich, *Weakly Connected Neural Networks* (Springer-Verlag, New York, 1997); S. H. Strogatz, From Kuramoto to Crawford: exploring the onset of synchronization in populations of coupled oscillators, *Physica D: Nonlinear Phenomena* **143**, 1 (2000); E. M. Izhikevich, *Dynamical Systems in Neuroscience: The Geometry of Excitability and Bursting* (The MIT Press, Cambridge, MA, 2007).
- [6] K. Yoshimura and K. Arai, Phase reduction of stochastic limit cycle oscillators, *Physical Review Letters* **101**, 154101 (2008); J. Teramae, H. Nakao, and G. B. Ermentrout, Stochastic phase reduction for a general class of noisy limit cycle oscillators, *Physical Review Letters* **102**, 194102 (2009); D. S. Goldobin, J. Teramae, H. Nakao, and G. B. Ermentrout, Dynamics of limit-cycle oscillators subject to general noise, *ibid.* **105**, 154101 (2010).
- [7] H. Nakao, T. Yanagita, and Y. Kawamura, Phase description of stable limit-cycle solutions in reaction-diffusion systems, *Procedia IUTAM* **5**, 227 (2012); Phase-reduction approach to synchronization of spatiotemporal rhythms in reaction-diffusion systems, *Physical Review X* **4**, 021032 (2014).
- [8] E. F. Stone, Frequency entrainment of a phase coherent attractor, *Physics Letters A* **163**, 367 (1992); M. G. Rosenblum, A. S. Pikovsky, and J. Kurths, Phase synchronization of chaotic oscillators, *Physical Review Letters* **76**, 1804 (1996).
- [9] K. Josić and D. J. Mar, Phase synchronization of chaotic systems with small phase diffusion, *Physical Review E* **64**, 056234 (2001).
- [10] A. Pikovsky, M. Zaks, M. Rosenblum, G. Osipov, and J. Kurths, Phase synchronization of chaotic oscillations in terms of periodic orbits, *Chaos: An Interdisciplinary Journal of Nonlinear Science* **7**, 680 (1997).
- [11] M. Beck and K. Josić, A geometric theory of chaotic

- phase synchronization, *Chaos: An Interdisciplinary Journal of Nonlinear Science* **13**, 247 (2003).
- [12] J. D. Farmer, E. Ott, and J. A. Yorke, The dimension of chaotic attractors, *Physica D: Nonlinear Phenomena* **7**, 153 (1983); M. Blank and L. Bunimovich, Multicomponent dynamical systems: SRB measures and phase transitions, *Nonlinearity* **16**, 387 (2003).
- [13] E. N. Lorenz, Deterministic nonperiodic flow, *Journal of the Atmospheric Sciences* **20**, 130 (1963); E.-H. Park, M. A. Zaks, and J. Kurths, Phase synchronization in the forced Lorenz system, *Physical Review E* **60**, 6627 (1999).
- [14] See Supplemental Material at [URL will be inserted by publisher] for details of the numerical demonstration carried out in this article.
- [15] We use a moving average filter to produce an effect similar to that produced by the fast fluctuations in ψ that were ignored in the derivation of Eq. (13). (See the above-mentioned Supplemental Material for further discussion.)
- [16] H. Fujisaka, T. Yamada, G. Kinoshita, and T. Kono, Chaotic phase synchronization and phase diffusion, *Physica D: Nonlinear Phenomena* **205**, 41 (2005).

On the phase description of chaotic oscillators —Supplemental Material—

Takashi Imai,¹ Hiromichi Suetani,^{2,3} and Toshio Aoyagi¹

¹*Graduate School of Informatics, Kyoto University, Kyoto 606-8501, Japan*

²*Faculty of Science and Technology, Oita University, Oita 870-1192, Japan*

³*Rhythm-Based Brain Information Processing Unit,*

RIKEN Center for Brain Science, Saitama 351-0198, Japan

(Dated: May 12, 2022)

In this supplemental material, we present additional numerical results and explain details of the numerical demonstration carried out in the main article.

The analysis presented in the main article suggests that the MAPO (16) with the map (13) accurately describes the rhythmic properties (such as the average frequency) of the original chaotic oscillator. Here, we demonstrate the validity of this description through consideration of numerical examples.

As a first example, we consider the following Rössler oscillator [S1] driven by a weak sinusoidal perturbation:

$$\begin{aligned} \dot{x} &= -y - z + \varepsilon \sin \Omega t, \\ \dot{y} &= x + ay, \quad \dot{z} = b + z(x - c), \end{aligned} \quad (\text{S1})$$

with the parameter values $a = 0.2$, $b = 0.2$, and $c = 5.7$. Does the MAPO model [Eqs. (13) and (16)] accurately produce the Arnold tongue for this system? The Arnold tongue can be constructed using the MAPO model by calculating the range of Ω in which there exists at least one value of ψ satisfying the conditions

$$f_\varepsilon(\psi) = 0 \quad \text{and} \quad \frac{df_\varepsilon}{d\psi}(\psi) < 0, \quad (\text{S2})$$

where $f_\varepsilon(\psi)$ denotes the right-hand side of Eq. (14)—i.e.,

$$f_\varepsilon(\psi) = \delta\omega(\psi; \varepsilon) + \varepsilon G(\psi; \varepsilon).$$

To obtain $\delta\omega$ and G , we adopt the surface of section depicted in Fig. S1(a), which is one of the optimal isophases (constructed using the method of Ref. [S2]) of the unperturbed system. With this surface of section, the variation in the return time [see Fig. S1(b)] is sufficiently small that Eq. (12) provides an accurate approximation of Eq. (9). Using numerical simulations, we can easily evaluate $T(i)$, $R_r(T(i); i)$, $\Phi(T(i); i)$, $\Upsilon(t; i)$, and $\zeta(\phi; i)$. This allows us to calculate $\delta\omega$ and G defined in Eqs. (15). With this treatment, the MAPO model produces the Arnold tongue depicted in Fig. S1(c). Except in several isolated regions, the discrepancy between the form of the Arnold tongue derived from the MAPO model and that derived from the original model is small. The only significant discrepancy between the two consists of several horizontal spikes in the former [e.g., near $(\varepsilon, \Omega) = (0.021, 1.077)$].

To understand the appearance of the horizontal spikes, let us consider Fig. S1(d), which plots the instantaneous

frequency difference, $\delta\omega$, and the coupling function, G , on one of these spikes. The curves in this figure have jumps at several values of ψ . These jumps dramatically extend the range of Ω in which there exists at least one value of ψ satisfying the conditions (S2). This leads to the emergence of the spike. A closer investigation reveals that these jumps correspond to the values of ψ at which narrow periodic windows appear in the R -dynamics (13). The spikes reflect these large changes occurring in narrow parameter ranges.

The spikes are not observed in the Arnold tongue derived from the full model. This is because, in the full model, the phase difference ψ fluctuates slightly on the time scale of the R -dynamics, and consequently R does not remain confined to these narrow windows. This observation suggests that the fast fluctuations in ψ play a key role in smoothing the frequency change.

To produce an effect similar to that caused by the fast fluctuations in ψ , we can utilize a moving average filter. By applying this filter to $\delta\omega$ and G , the MAPO model is adjusted so that it provides a more accurate approximation [see Fig. S1(e)].

The remaining slight difference between the Arnold tongue obtained from the full model and that obtained from the MAPO model can be attributed to the anomalous enhancement of the diffusion coefficient discussed in Ref. [S3]. This enhancement occurs near the point at which CPS breaks down and weakens the system's periodicity in that region. Because the MAPO model is constructed assuming strong periodicity of the system, as this periodicity weakens, the discrepancy between the forms of the Arnold tongue derived from the full model and the MAPO model increases. However, as long as it is not too large, the error inherent in the form derived from the MAPO model does not prevent us from obtaining an accurate understanding of the global structure of the tongue, because this error is localized in the region near the point at which CPS breaks down.

As a second example, we consider the Lorenz oscillator driven by weak sinusoidal perturbation given in Eqs. (17), with the parameter values $\sigma = 10$, $\beta = 8/3$, and $\rho = 210$. We use the flat surface depicted in Fig. S2(a) as the surface of section. Although this surface was not determined

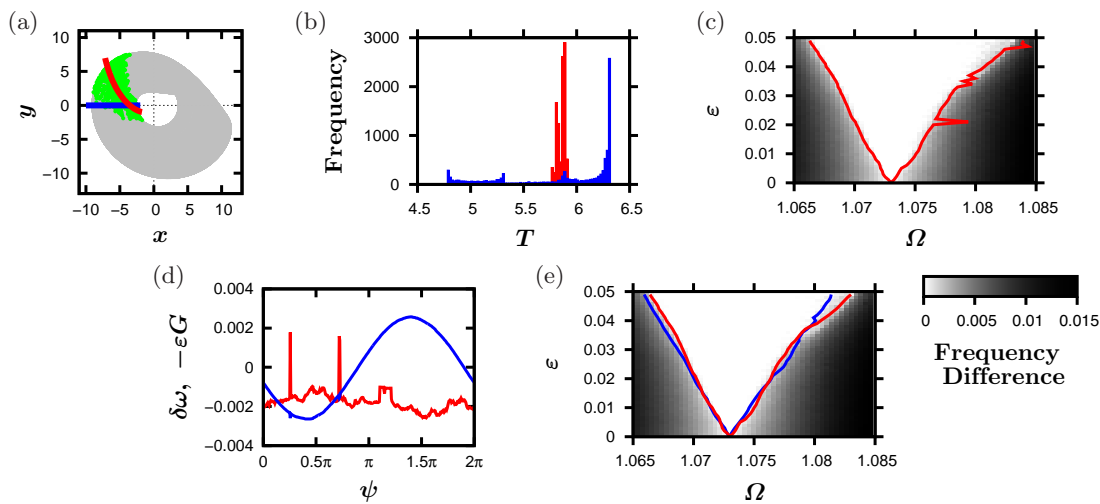


FIG. S1. Numerical results for the Rössler oscillator. (a) The trajectory (gray curve), the stroboscopic set [S2] (green dots), and the adopted surface of section (red curve). The blue line segment represents a simpler surface of section ($x < 0, y = 0$). These surfaces of section yield the return time distributions plotted in (b), where the red and blue histograms depict the distributions for the former and latter surfaces of section, respectively. (c) The difference between the frequencies of the periodic driving and the driven system observed in the full model. The red curve indicates the edge of the Arnold tongue derived from the MAPO model (i.e., the boundary of the (ε, Ω) -region in which CPS occurs in the MAPO model). (d) The instantaneous frequency difference $\delta\omega$ (red curve) and the coupling function G (blue curve) at $(\varepsilon, \Omega) = (0.021, 1.077)$. By preprocessing these quantities using a moving average filter, we obtained a more accurate approximation (e). In this figure, for reference, the blue curve indicates the edge of the Arnold tongue obtained by using the other surface of section.

through a careful optimization procedure, with it, the variation of the return time is indeed small, varying by only approximately $\pm 2\%$ [see Fig. S2(b)]. (This is close to the same as the variation observed in our investigation of the Rössler oscillator, discussed above, in which we used an optimal isophase.) With this small variation, the form of the Arnold tongue derived from the MAPO model in this case again deviates only slightly from that derived from the full model, as shown in Fig. S2(c).

The Arnold tongue for the Lorenz oscillator (17) exhibits an abrupt extension of the synchronization range along the Ω -axis at $\varepsilon = \varepsilon_c \approx 0.46$. This extension, like the spikes in the case of the Rössler oscillator, also reflects the appearance of periodic windows in the R -dynamics. The difference between the present situation and that for the Rössler oscillator is that in the present situation, the periodic windows are so wide that despite the fluctuations of ψ , R remains confined to these windows for some time, and hence these windows have a strong effect even on the behavior of the full model. Note that the MAPO model accurately approximates the frequency in the regions both above and below $\varepsilon = \varepsilon_c$. This indicates that

the MAPO model properly inherits the perturbation dependence of the non-phase variables from the full model. This inheritance results from the fact that $\bar{\omega}$ and $\bar{\zeta}$ in the phase oscillator (16) depend on the natural measure μ_i ; when the periodic driving triggers a qualitative change in the behavior of R , this change leads to large changes in μ_i , and thus in the characteristics of the phase oscillator (16). In this way, the MAPO model successfully incorporates the dynamics of the non-phase variables existing in the system.

-
- [S1] O. E. Rössler, An equation for continuous chaos, *Physics Letters A* **57**, 397 (1976).
 - [S2] J. T. C. Schwabedal, A. Pikovsky, B. Kralemann, and M. Rosenblum, Optimal phase description of chaotic oscillators, *Physical Review E* **85**, 026216 (2012).
 - [S3] H. Fujisaka, T. Yamada, G. Kinoshita, and T. Kono, Chaotic phase synchronization and phase diffusion, *Physica D: Nonlinear Phenomena* **205**, 41 (2005).

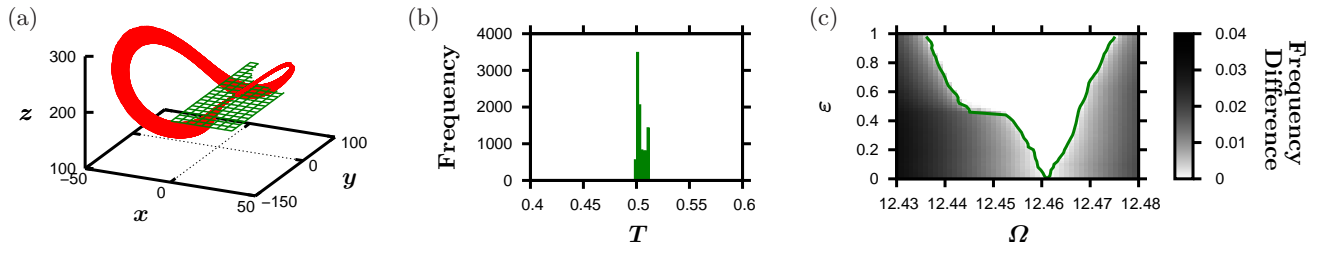


FIG. S2. Numerical results for the Lorenz oscillator. (a) The trajectory (red curve) and the adopted surface of section (green mesh surface). This surface of section yields the return time distribution plotted in (b). (c) The difference between the frequencies of the periodic driving and the driven system observed in the full model. The green curve indicates the edge of the Arnold tongue obtained from the MAPO model using the smoothed $\delta\omega$ and G .